

**NATIONAL ADVISORY COMMITTEE
FOR AERONAUTICS**

REPORT No. 745

**HIGH-SPEED TESTS OF CONVENTIONAL
RADIAL-ENGINE COWLINGS**

By RUSSELL G. ROBINSON and JOHN V. BECKER



1942

AERONAUTIC SYMBOLS

1. FUNDAMENTAL AND DERIVED UNITS

	Symbol	Metric		English	
		Unit	Abbrevia- tion	Unit	Abbrevia- tion
Length.....	l	meter.....	m	foot (or mile).....	ft (or mi)
Time.....	t	second.....	s	second (or hour).....	sec (or hr)
Force.....	F	weight of 1 kilogram.....	kg	weight of 1 pound.....	lb
Power.....	P	horsepower (metric).....		horsepower.....	hp
Speed.....	V	{kilometers per hour.....	kph	miles per hour.....	mph
		{meters per second.....	mps	feet per second.....	fps

2. GENERAL SYMBOLS

W	Weight = mg	ν	Kinematic viscosity
g	Standard acceleration of gravity = 9.80665 m/s ² or 32.1740 ft/sec ²	ρ	Density (mass per unit volume) Standard density of dry air, 0.12497 kg-m ⁻⁴ -s ² at 15° C and 760 mm; or 0.002378 lb-ft ⁻⁴ sec ²
m	Mass = $\frac{W}{g}$		Specific weight of "standard" air, 1.2255 kg/m ³ or 0.07651 lb/cu ft
I	Moment of inertia = mk^2 . (Indicate axis of radius of gyration k by proper subscript.)		
μ	Coefficient of viscosity		

3. AERODYNAMIC SYMBOLS

S	Area	i_w	Angle of setting of wings (relative to thrust line)
S_w	Area of wing	i_t	Angle of stabilizer setting (relative to thrust line)
G	Gap	Q	Resultant moment
b	Span	Ω	Resultant angular velocity
c	Chord	R	Reynolds number, $\rho \frac{Vl}{\mu}$ where l is a linear dimen- sion (e.g., for an airfoil of 1.0 ft chord, 100 mph, standard pressure at 15° C, the corresponding Reynolds number is 935,400; or for an airfoil of 1.0 m chord, 100 mps, the corresponding Reynolds number is 6,865,000)
A	Aspect ratio, $\frac{b^2}{S}$	α	Angle of attack
V	True air speed	ϵ	Angle of downwash
q	Dynamic pressure, $\frac{1}{2}\rho V^2$	α_0	Angle of attack, infinite aspect ratio
L	Lift, absolute coefficient $C_L = \frac{L}{qS}$	α_i	Angle of attack, induced
D	Drag, absolute coefficient $C_D = \frac{D}{qS}$	α_a	Angle of attack, absolute (measured from zero- lift position)
D_0	Profile drag, absolute coefficient $C_{D_0} = \frac{D_0}{qS}$	γ	Flight-path angle
D_i	Induced drag, absolute coefficient $C_{D_i} = \frac{D_i}{qS}$		
D_p	Parasite drag, absolute coefficient $C_{D_p} = \frac{D_p}{qS}$		
C	Cross-wind force, absolute coefficient $C_C = \frac{C}{qS}$		

REPORT No. 745

**HIGH-SPEED TESTS OF CONVENTIONAL
RADIAL-ENGINE COWLINGS**

By **RUSSELL G. ROBINSON** and **JOHN V. BECKER**

Langley Memorial Aeronautical Laboratory
Langley Field, Va.

NATIONAL ADVISORY COMMITTEE FOR AERONAUTICS

HEADQUARTERS, 1500 NEW HAMPSHIRE AVENUE NW., WASHINGTON, D. C.

Created by act of Congress approved March 3, 1915, for the supervision and direction of the scientific study of the problems of flight (U. S. Code, title 50, sec. 151). Its membership was increased to 15 by act approved March 2, 1929. The members are appointed by the President, and serve as such without compensation.

JEROME C. HUNSAKER, Sc. D., *Chairman*,
Cambridge, Mass.

GEORGE J. MEAD, Sc. D., *Vice Chairman*,
Washington, D. C.

CHARLES G. ABBOT, Sc. D.,
Secretary, Smithsonian Institution.

HENRY H. ARNOLD, Lieut. General, United States Army,
Commanding General, Army Air Forces, War Department.

LYMAN J. BRIGGS, Ph. D.,
Director, National Bureau of Standards.

W. A. M. BURDEN,
Special Assistant to the Secretary of Commerce.

VANNEVAR BUSH, Sc. D., Director,
Office Scientific Research and Development,
Washington, D. C.

WILLIAM F. DURAND, Ph. D.,
Stanford University, Calif.

O. P. ECHOLS, Major General, United States Army, Com-
manding General, The Matériel Command, Army Air
Forces, War Department.

SYDNEY M. KRAUS, Captain, United States Navy, Bureau of
Aeronautics, Navy Department.

FRANCES W. REICHELDERFER, Sc. D.,
Chief, United States Weather Bureau.

JOHN H. TOWERS, Rear Admiral, United States Navy,
Chief, Bureau of Aeronautics, Navy Department.

EDWARD WARNER, Sc. D.,
Civil Aeronautics Board,
Washington, D. C.

ORVILLE WRIGHT, Sc. D.,
Dayton, Ohio.

THEODORE P. WRIGHT, Sc. D.,
Asst. Chief, Aircraft Branch,
War Production Board.

GEORGE W. LEWIS, *Director of Aeronautical Research*

JOHN F. VICTORY, *Secretary*

HENRY J. E. REID, *Engineer-in-Charge, Langley Memorial Aeronautical Laboratory, Langley Field, Va.*

SMITH J. DEFRAANCE, *Engineer-in-Charge, Ames Aeronautical Laboratory, Moffett Field, Calif.*

EDWARD R. SHARP, *Administrative Officer, Aircraft Engine Research Laboratory, Cleveland Airport, Cleveland, Ohio*

TECHNICAL COMMITTEES

AERODYNAMICS
POWER PLANTS FOR AIRCRAFT

AIRCRAFT MATERIALS
AIRCRAFT STRUCTURES

INVENTIONS & DESIGNS
OPERATING PROBLEMS

Coordination of Research Needs of Military and Civil Aviation

Preparation of Research Programs

Allocation of Problems

Prevention of Duplication

Consideration of Inventions

LANGLEY MEMORIAL AERONAUTICAL LABORATORY

LANGLEY FIELD, VA.

AMES AERONAUTICAL LABORATORY

MOFFETT FIELD, CALIF.

AIRCRAFT ENGINE RESEARCH LABORATORY

CLEVELAND AIRPORT, CLEVELAND, OHIO

Conduct, under unified control, for all agencies, of scientific research on the fundamental problems of flight.

OFFICE OF AERONAUTICAL INTELLIGENCE

WASHINGTON, D. C.

Collection, classification, compilation, and dissemination of
scientific and technical information on aeronautics

REPORT No. 745

HIGH-SPEED TESTS OF CONVENTIONAL RADIAL-ENGINE COWLINGS*

By RUSSELL G. ROBINSON and JOHN V. BECKER

SUMMARY

The drag characteristics of eight radial-engine cowlings have been determined over a wide speed range in the NACA 8-foot high-speed wind tunnel. The pressure distribution over all cowlings was measured, to and above the speed of the compressibility burble, as an aid in interpreting the force tests. One-fifth-scale models of radial-engine cowlings on a wing-nacelle combination were used in the tests.

The speed at which the effective nacelle drag abruptly increased owing to the compressibility burble was found to vary from 310 miles per hour for one of the existing cowling shapes to 480 miles per hour for the best shape developed as a result of the present investigation. The corresponding speeds at 30,000 feet altitude in a standard atmosphere ($-48^{\circ} F$) are 280 and 430 miles per hour, respectively. Correlation between the peak negative pressure on the surface of a cowling and the critical speed of the cowling was established. The speed at which the effective nacelle drag abruptly increased was found to be equal to, or slightly greater than, the flight speed at which the speed of sound is reached locally on the cowling. The criterion for the design of conventional cowlings with high critical speeds appears to be small negative pressures of uniform distribution over the cowling nose, indicative of local velocities that exceed the general stream velocity by a minimum amount. The cowlings developed on this principle had not only the highest critical speeds but also the lowest drags throughout the entire speed range and had greater useful ranges of angle of attack.

INTRODUCTION

Experimental work on bodies of many shapes at high speeds has shown that for each shape a speed is reached at which a compressibility burble occurs, causing an abrupt increase in drag and causing, on lifting bodies, a loss of lift and a marked increase in pitching moment. The nature of the compressibility burble is described in reference 1, where it is shown that a compression shock forms on a body when the local airspeed over any part of the body exceeds the local speed of sound. The flight speed at which the local speed of sound is reached is therefore the limiting speed below which the aerodynamic characteristics of a body may be expected to vary in a regular manner and is termed "critical" speed. This critical speed, dependent on the shape and the lift of the body, usually lies between 0.4 and 0.9 times the speed of sound, or 305 to 686 miles per hour in standard

sea-level atmosphere. The compression shock occurring after the critical speed is reached involves a sudden, rather than a gradual, retardation of the air that has reached supersonic speeds near the surface of the body and results in a dissipation of energy. The source of the increased drag observed at the compressibility burble is the compression shock, and the excess drag is due to the conversion of a considerable amount of the airstream kinetic energy into heat at the compression shock. The drag increases still further at speeds above the compressibility burble because both the intensity (pressure drop) and the extent of the shock measured perpendicular to the body surface increase with increasing speed. It is also known that the presence of a compression shock tends to aggravate separation of the flow over the trailing portion of a body and thereby further increases the drag.

The effect of the drag increase caused by the compression shock on airplane performance is practically to limit the maximum speed of an airplane to the lowest critical speed of any of its large component parts because of the excessive power required to overcome the drag at higher speeds. The desirability of determining the critical speeds of component parts of an airplane, especially those contributing the most drag and those with the lowest critical speed, is apparent.

Reference 2 supports the reasoning that blunt bodies or bodies of high curvature (for example, circular cylinders as compared with airfoil sections) have the lowest critical speeds because the maximum local airspeed near the surface of such bodies reaches the local speed of sound at a comparatively low free-stream speed. Radial-engine cowlings fall in this class and there are pressure-distribution results available to indicate the magnitude of the maximum speed over a number of typical practical cowlings. The results of experimental work on full-scale cowlings tested on an operating engine are given in reference 3. The pressure-distribution data from that reference indicate that two of the cowlings had local speeds over the nose portion approximately twice the magnitude of the free-stream speed. The critical speed of such cowlings (as predicted by the known peak negative pressure and the relation, presented in reference 4, between the peak pressure and the critical speed) is about 300 miles per hour. Reference 3 also shows the direct effect of curvature of the cowling nose on the peak negative pressure, and hence on maximum local speed over the cowling. This effect suggests increasing the critical speed

of a radial-engine cowling by a proper distribution of the curvature.

Reference 3 further shows that the effect of a propeller operating at the high-speed or the cruising condition does not appreciably alter the peak negative pressure over a cowling in the slipstream. This result is to be expected because at high speeds the propeller slip is small compared with the forward speed. The critical speed of a cowling under service operating conditions

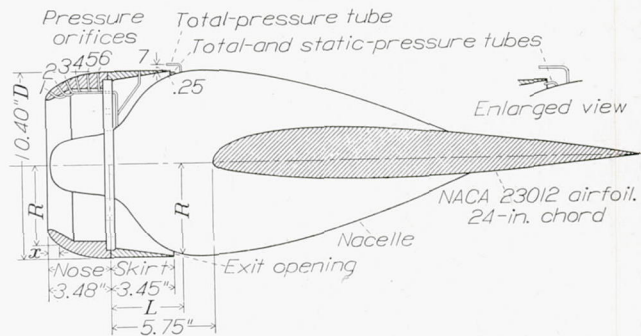


FIGURE 1.—Assembly of wing, nacelle, and cowling. Nose C, skirt 1.

may therefore be determined quite accurately by the use of a model without a propeller.

The purpose of the present investigation was to determine in the high-speed range the merit of models of five full-scale cowlings and new cowling shapes developed from the test results of the first five. Results of the tests were to be correlated to allow the prediction of the compressibility burble from low-speed pressure measurements. The tests were conducted in May 1937 at Langley Memorial Aeronautical Laboratory.

APPARATUS AND METHOD

The NACA 8-foot high-speed wind tunnel in which the investigation was carried out is a single-return,

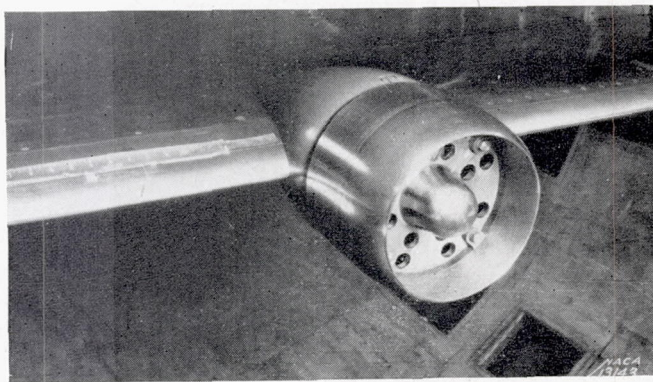


FIGURE 2.—Wing-nacelle combination. Nose 1, skirt 1.

circular, closed-throat tunnel. The flow in the test section has been found by surveys to be satisfactorily steady and uniform both in speed and direction. The airspeed is continuously controllable from 75 to more than 500 miles per hour. The turbulence, as determined by sphere tests (reference 5), is approximately equivalent to that of free air.

The radial-engine cowlings were mounted on a nacelle

which was mounted centrally on a wing of 2-foot chord and NACA 23012 section. The wing completely spanned the test section of the tunnel. The cowlings and the nacelle were one-fifth the size of the full-scale cowlings and nacelle reported in reference 3. The wing was metal-covered, unpainted, and aerodynamically smooth; that is, further polishing would

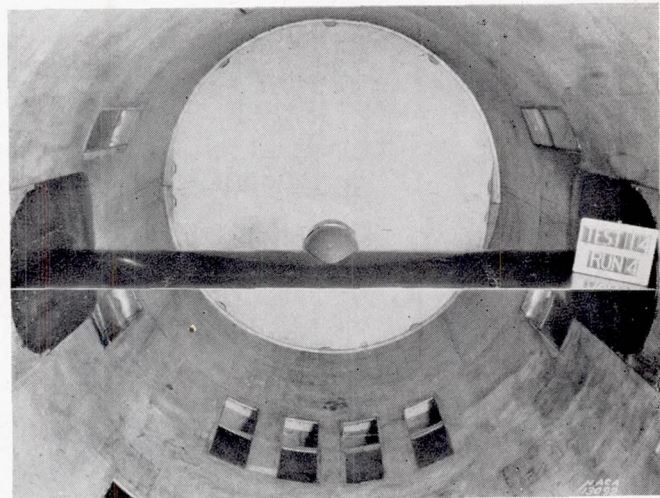


FIGURE 3.—Rear view of wing-nacelle combination mounted in the tunnel.

produce no decrease in profile drag. Figure 1 is a cross-sectional view through the center of the wing-nacelle combination. A general view of the nacelle with cowling nose 1 and skirt 1 is shown in figure 2. Figure 3 shows the wing-nacelle assembly mounted in the tunnel.

One-fifth-scale (10.40-in. diameter) cowling models

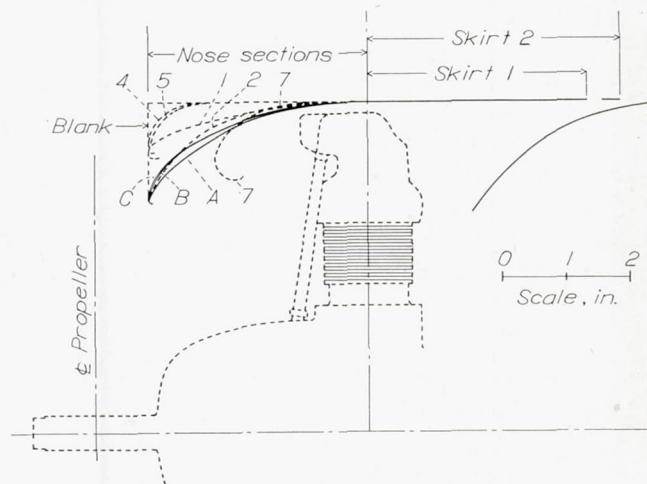


FIGURE 4.—Cowling profiles.

were chosen as the largest that could be used with the 2-foot-chord wing and still maintain normal wing-nacelle proportions. The ratio

$$\frac{\text{cowling diameter}}{\text{wing chord}} = 0.43$$

for the model is somewhat larger than for average practice but is within the range of present-day instal-

lations. The center line of the nacelle lay on the chord line of the wing. The fore-and-aft position of the nacelle was such as to locate the propeller, had there been one, 40 percent of the wing chord ahead of the leading edge.

The five cowling-nose shapes (fig. 4) scaled down from the corresponding full-scale cowlings employed in the investigation reported in reference 3 are designated by the numbers used in that investigation. Nose 1 was modified progressively by cutting back to larger radii at the leading edge. Noses A, B, and C were designed as the tests progressed. They have the same over-all dimensions as nose 2 but have different intermediate ordinates. Figure 5 presents photographs of nose 5 and nose C. A blank nose with a square corner and the same over-all dimensions as nose 2 was also tested. Table I gives the ordinates for all the cowling noses tested.

TABLE I.—VALUES OF R IN INCHES FOR EIGHT MODEL NOSES OF 10.40-INCH DIAMETER COWLING

[See figs. 1 and 4]

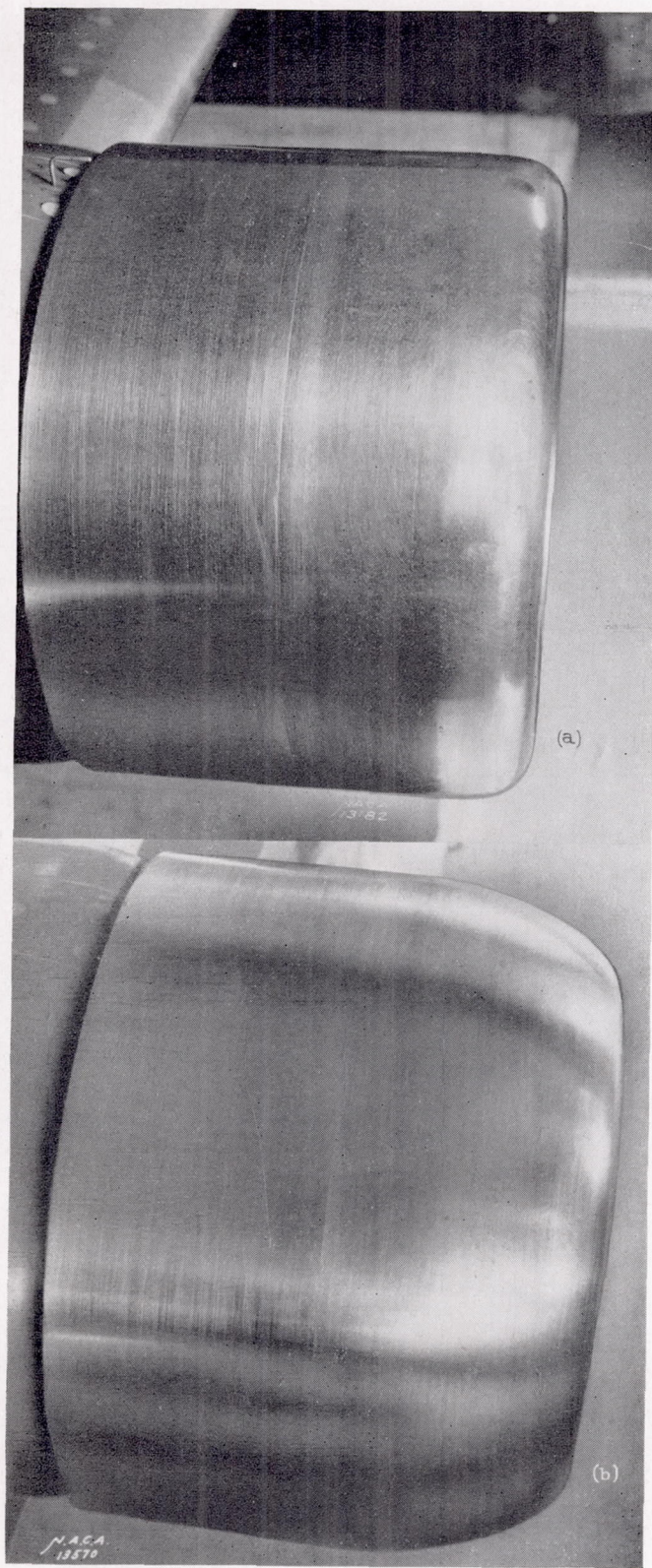
x (in.)	Nose								
	1	2	4	5	7		A	B	C
					Out- side	In- side			
0.00	4.40	3.64	4.48	4.36	4.29	4.29	3.64	3.64	3.64
.05	4.50	3.79	4.75	4.61	4.47	4.13	3.76	3.87	3.93
.10	4.53	3.88	4.84	4.70	4.56	4.06	3.84	3.97	4.02
.20	4.59	4.05	4.96	4.88	4.68	4.00	3.96	4.11	4.15
.40	4.70	4.32	5.09	5.05	4.87	3.98	4.16	4.31	4.33
.60	4.79	4.52	5.15	5.13	4.98	---	4.34	4.47	4.48
.80	4.85	4.67	5.18	5.17	5.07	---	4.48	4.59	4.59
1.00	4.91	4.79	5.19	5.18	5.13	---	4.60	4.70	4.70
1.20	4.96	4.88	5.20	5.19	5.16	---	4.71	4.80	4.78
1.40	5.00	4.96	5.20	5.20	5.18	---	4.81	4.87	4.86
1.60	5.04	5.03	5.20	5.20	5.19	---	4.90	4.94	4.96
2.00	5.10	5.11	5.20	5.20	5.20	---	5.03	5.04	5.05
2.40	5.14	5.14	5.20	5.20	5.20	---	5.12	5.12	5.13
2.80	5.18	5.18	5.20	5.20	---	---	5.18	5.17	5.18
3.20	5.20	5.20	5.20	5.20	---	---	5.20	5.19	5.20
3.23	5.20	5.20	5.20	5.20	---	---	5.20	5.20	5.20
3.48	5.20	5.20	5.20	5.20	---	---	5.20	5.20	5.20

Two cowling skirts were employed in the investigation. Ordinates of the nacelle, which is similar to nacelle 2 of reference 3, are given in table II.

TABLE II.—NACELLE-MODEL ORDINATES

[See figs. 1 and 4]

L (in.)	R (in.)	L (in.)	R (in.)
0.00	1.94	4.25	5.12
.25	2.02	4.75	5.16
.65	2.30	5.25	5.17
1.05	2.69	6.25	5.11
1.25	2.92	7.25	5.01
1.45	3.18	8.25	4.86
1.65	3.47	10.25	4.47
1.85	3.75	12.25	3.93
2.05	3.98	14.25	3.30
2.25	4.17	16.25	2.56
2.65	4.48	18.25	1.75
3.05	4.73	19.25	1.31
3.45	4.92	20.25	.87
3.85	5.04		



(a) Nose 5.
(b) Nose C.

FIGURE 5.—Model cowlings.

All the cowlings were tested with a controlled amount of cooling air through them. A flat baffle plate with sixteen 15/16-inch holes simulated a baffled radial engine

of conductivity K (reference 3), or equivalent leak area, approximately 9 percent. The baffle plate was incidentally used to support the replaceable nose and skirt portions, which were of cast nickel-iron and were finished smooth and flush.

Cowling skirt 1 provided an exit-slot opening of 0.25 inch and a baffle-plate pressure drop, $\Delta p = 0.25q$. (Dynamic pressure $q = 1/2 \rho V^2$.) Cowling skirt 2 pro-

vided an exit opening of 0.11 inch (0.55 in. on full-scale engine cowling) and a value of Δp of $0.12q$.

The pressure distribution over the top of each cowling was measured at seven static-pressure orifices (fig. 1). The orifices were located according to the expected pressure distribution for the particular cowling; several tubes were located near the point of peak negative pressure. The locations are given in table III.

TABLE III.—LOCATION OF PRESSURE ORIFICES ON COWLINGS

[See fig. 1]

Nose	Orifice													
	1		2		3		4		5		6		7	
	x (in.)	R (in.)	x (in.)	R (in.)	x (in.)	R (in.)	x (in.)	R (in.)	x (in.)	R (in.)	x (in.)	R (in.)	x (in.)	R (in.)
1.....	0.01	4.41	0.04	4.49	0.23	4.62	0.80	4.85	1.60	5.04	2.75	5.17	5.18	5.20
2.....	.25	4.09	.70	4.60	1.16	4.86	1.70	5.05	2.25	5.13	3.00	5.19	5.18	5.20
4.....	0	4.50	.10	4.84	.25	4.99	.45	5.11	.69	5.17	2.00	5.20	5.18	5.20
5.....	.03	4.49	.20	4.88	.35	5.00	.50	5.11	.90	5.19	2.00	5.20	5.18	5.20
7.....	0	4.29	.10	4.56	.35	4.80	.65	5.01	1.00	5.13	1.50	5.19	5.18	5.20
A.....	.25	4.01	.70	4.40	1.16	4.67	1.70	4.91	2.25	5.08	3.00	5.19	5.18	5.20
B.....	.25	4.17	.70	4.53	1.16	4.78	1.70	4.97	2.25	5.09	3.00	5.18	5.18	5.20
C.....	.25	4.20	.70	4.54	1.16	4.76	1.70	4.96	2.25	5.10	3.00	5.19	5.18	5.20

A total-pressure tube was located above the cowling skirt near its trailing edge (see figs. 1 and 5) for detecting any loss, such as that of a compression shock, outside the boundary layer. A total-pressure tube and a static-pressure tube were placed in the center of the exit opening on the top side of the nacelle for measuring the airspeed and the total pressure in the exit opening.

All the cowlings were tested over a speed range extending from 115 miles per hour to a speed greater than the critical speed for each model at angles of attack of -1° and 0° . Owing to structural limitations of the wing, the maximum airspeed was limited to 425 miles per hour at 1° and to 275 miles per hour at 2° . Noses 1-f, 5, and B, which were considered representative of the several types investigated, were tested through a range of angles of attack of -3° to 6° at 230 miles per hour. All the models were tested with skirt 1; only nose 5 was tested with skirt 2.

The lift, the drag, and the pitching moment of the wing-nacelle-cowling combinations were measured at intervals of 30 miles per hour at the lower speeds and more frequently near the critical speeds. The characteristics of the wing alone were determined in the same way. Pressure measurements on the cowlings were made simultaneously with the force measurements.

RESULTS

Compressibility effects, such as those encountered at high speeds on the engine cowlings under consideration, are intimately connected with the nondimensional Mach number M in the same way that scale effects are connected with the Reynolds number R . Mach number

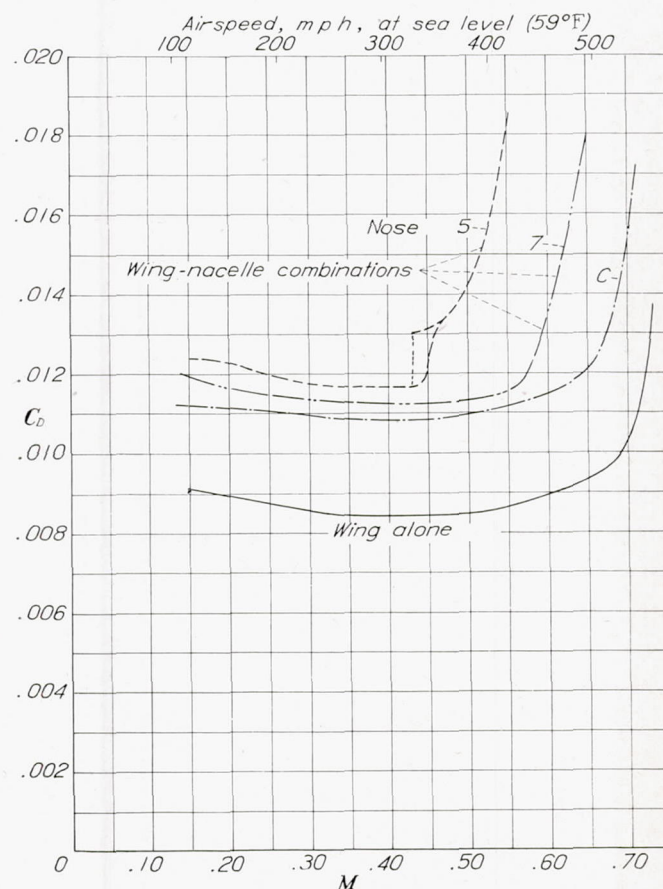


FIGURE 6.—Drag of wing and wing-nacelle combinations. Uncorrected for tunnel-wall effects. $\alpha = -1^\circ$.

M is the ratio of airspeed V to the speed of sound in the air a . Results in this report are plotted against M .

Given the temperature of the air, the airspeed corre-

sponding to a given Mach number M may be found from

$$V = Ma$$

and

$$a = 33.5\sqrt{460 + t}$$

where t is the temperature in Fahrenheit degrees and V and a are in miles per hour. In some cases, for ease in

with standard aeronautical practice. The results, as presented, then indicate directly all compressibility effects.

FORCE TESTS AND PRESSURE-DISTRIBUTION MEASUREMENTS

The results are presented in terms of nondimensional coefficients. Figure 6 shows the relative magnitude of the drag force of the wing alone and the wing-nacelle

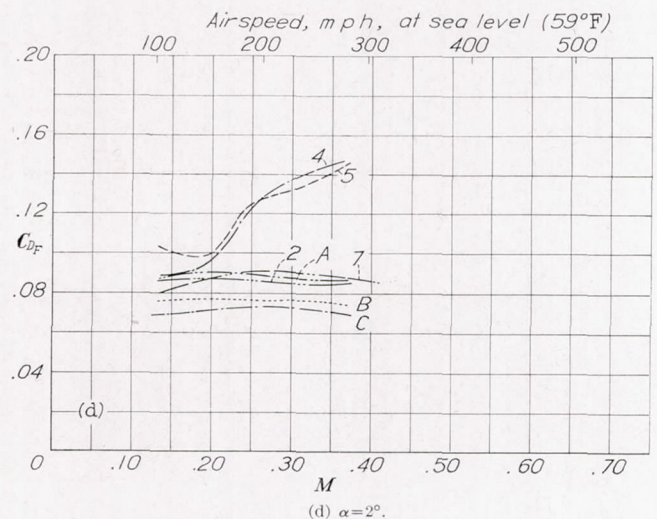
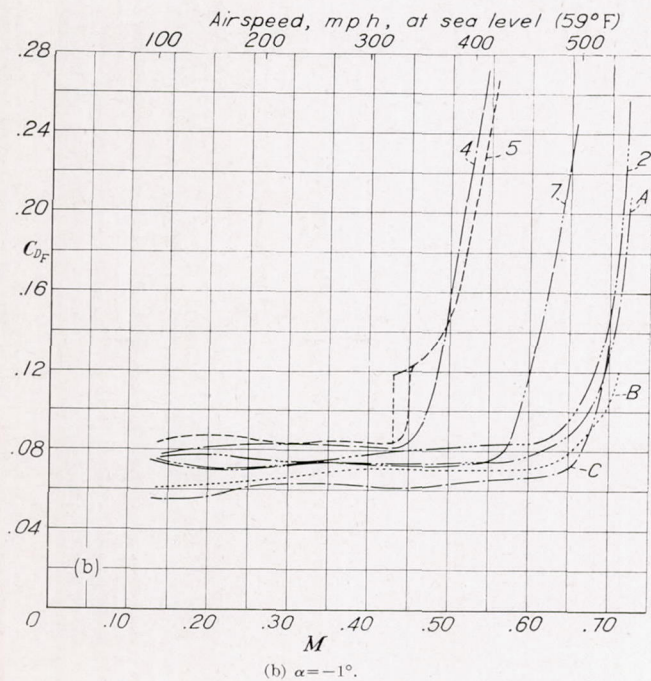
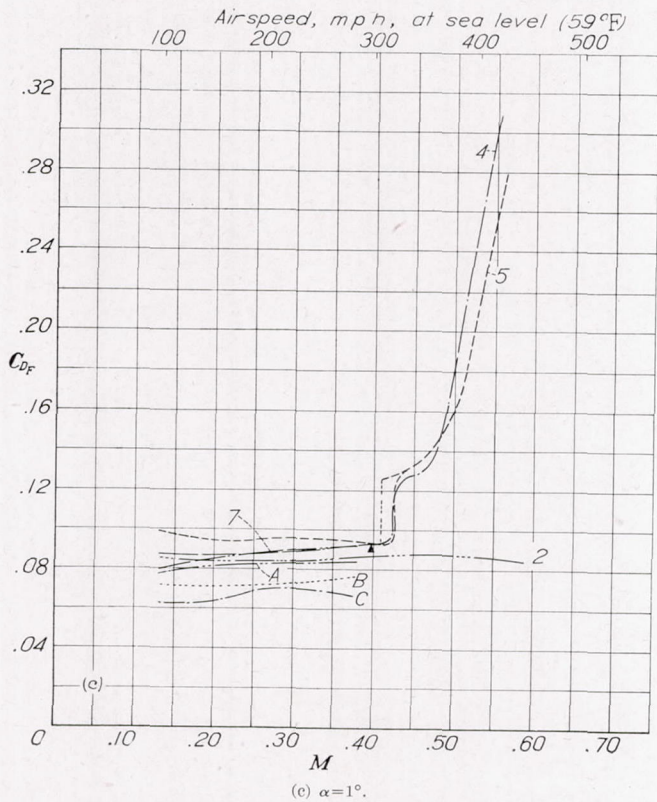
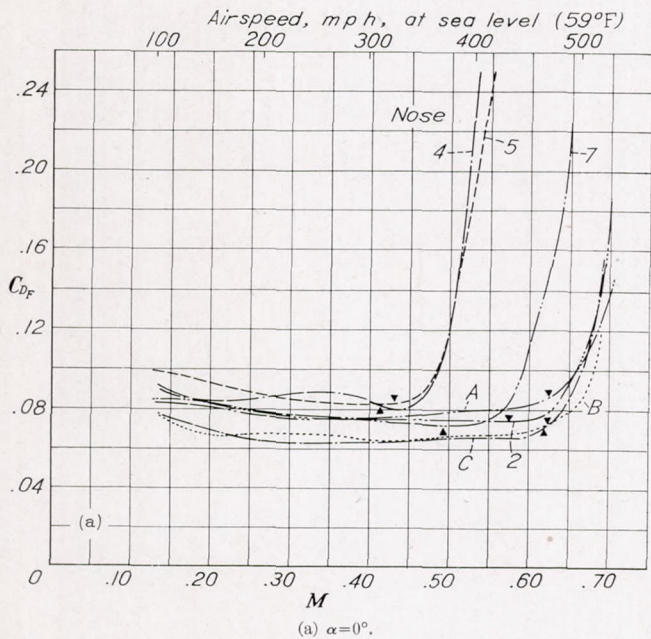


FIGURE 7.—Effective nacelle drag for various noses, skirt 1. The ticks indicate the critical M .

visualizing the magnitude of the speeds, a scale of airspeed for standard sea-level conditions ($t = 59^\circ F$, $a = 763$ mph) is included in the figures.

The drag coefficients and the pressure coefficients are computed using the dynamic pressure in accordance

combination (both uncorrected for tunnel-wall effects). The drag coefficients for this figure are based on wing area:

$$C_D = \frac{\text{drag of wing + nacelle}}{q \times 15.35}$$

For use in the comparison of the drags of various cowlings, an effective nacelle drag coefficient C_{DF} based on the frontal area of the cowling (0.590 sq ft) is used. This coefficient, of course, includes the drag and the interference of the nacelle. By definition:

$$C_{DF} = \frac{\text{effective nacelle drag}}{q \times 0.590} \\ = \frac{(\text{drag of wing + nacelle}) - (\text{drag of wing alone})}{q \times 0.590}$$

Effective nacelle drag coefficients for the cowling noses 2, 4, 5, 7, A, B, and C with skirt 1 are shown in figure 7.

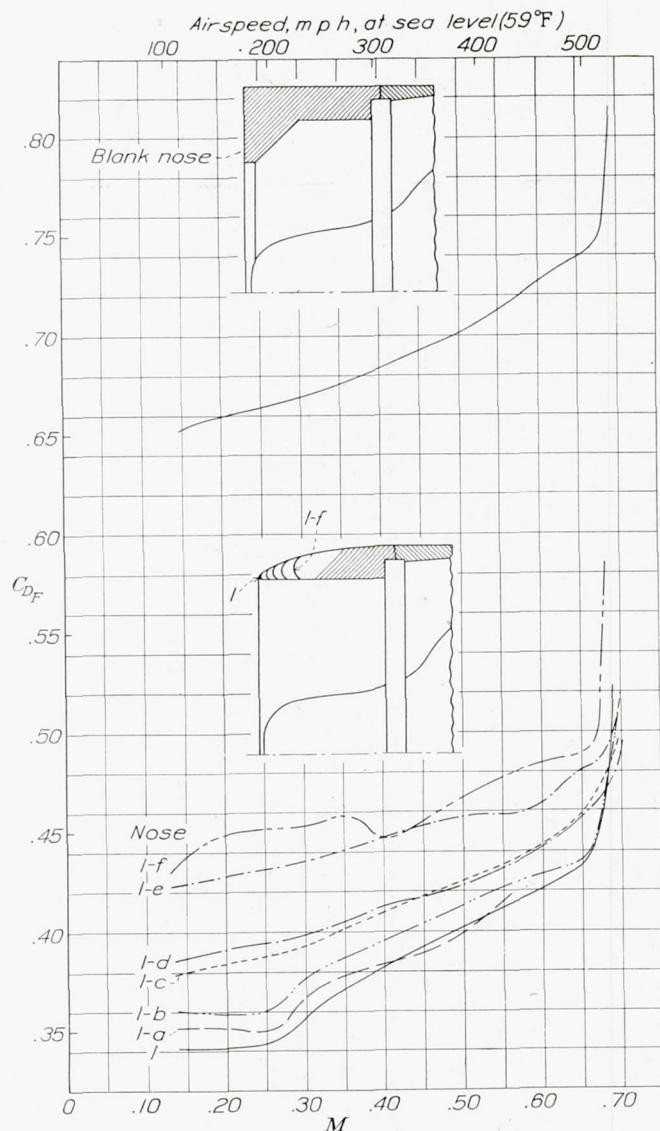


FIGURE 8.—Effective nacelle drag for nose 1, modifications to nose 1, and blank nose. $\alpha=0^\circ$.

The results obtained with nose 1 and with several modifications of nose 1, together with those for the square-corner blank nose, are shown in figure 8. Figure 9 shows the results of the test of nose 5 with skirt 2. The curves of effective nacelle drag were obtained from faired curves of the drag of the wing alone and the

drag of the wing-nacelle combination for the same angle of attack.

The pressure distribution over the nose section of a cowling is plotted in terms of the pressure coefficient P ,

$$P = \frac{p - p_\infty}{q}$$

where

p local static pressure

p_∞ static pressure in free stream

The value of P is then a measure of the local speed over the nose. Values of P equal to zero indicate a speed equal to the free-stream speed, positive values indicate less than free-stream speed; and negative values indicate more than free-stream speed.

The pressure-distribution diagrams for the models

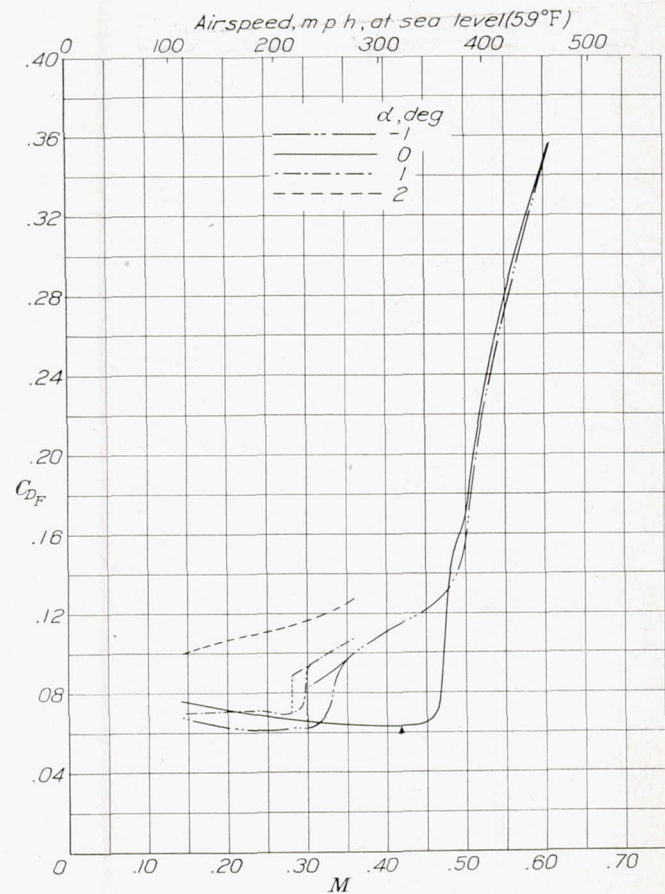


FIGURE 9.—Effective nacelle drag for nose 5, skirt 2. The tick indicates the critical M

at various angles of attack, at $M=0.30$, are shown in figure 10 (a) to (i). Figure 10 (j) shows the effect of the compressibility burble on the pressure distribution. Typical variation with M of the static pressure at each of the seven orifices is shown in figure 11 for noses 4, 7, and B at angles of attack of 0° and 1° . The loss in total pressure ΔH between the free stream and the total-pressure tube at the rear of the cowling is shown in figure 12 for noses 4, 5, 7, A, and B for angles of attack of 0° and 1° .

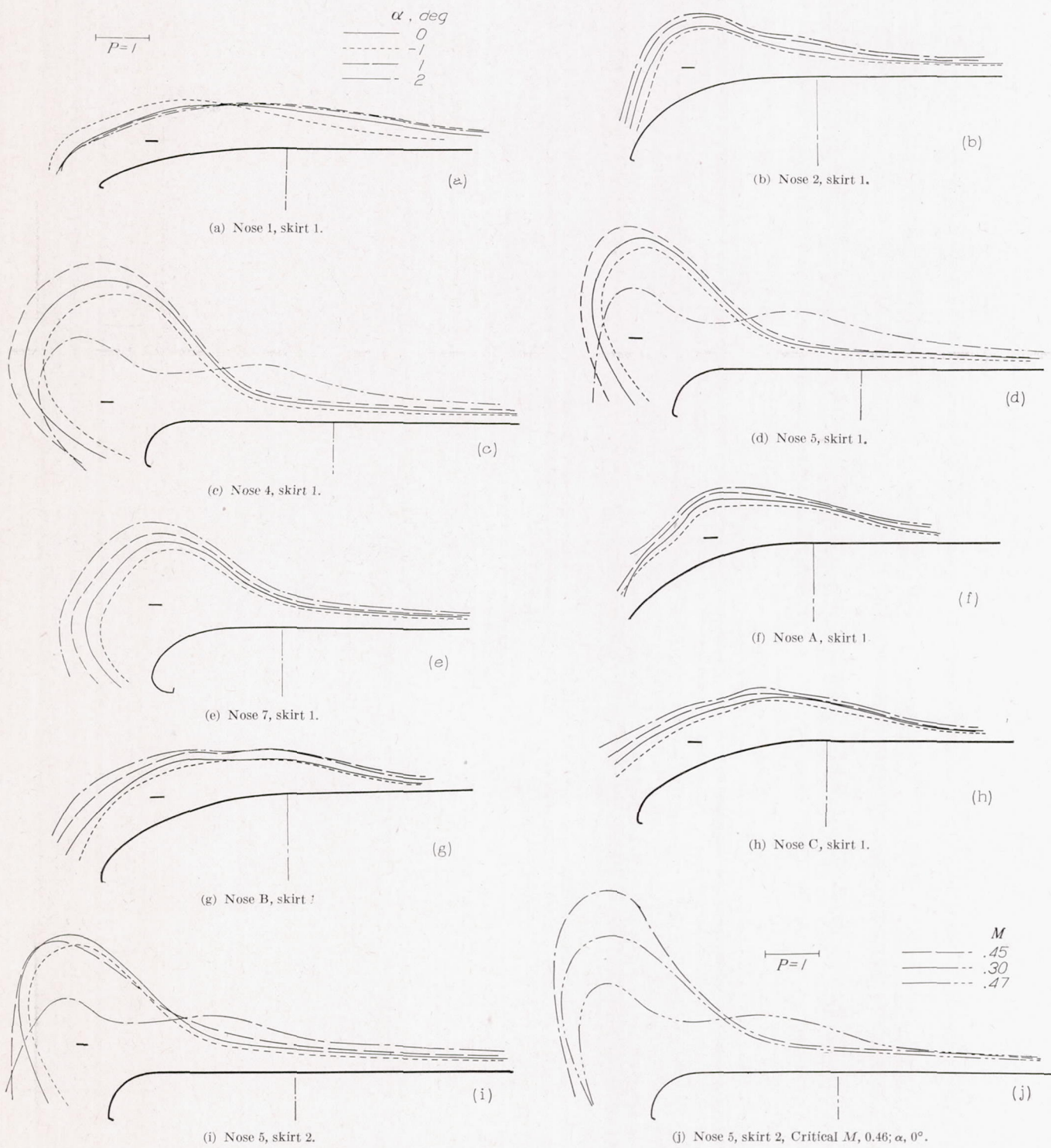


FIGURE 10.—Pressure distribution over top of cowlings. $M=0.30$, except as noted.

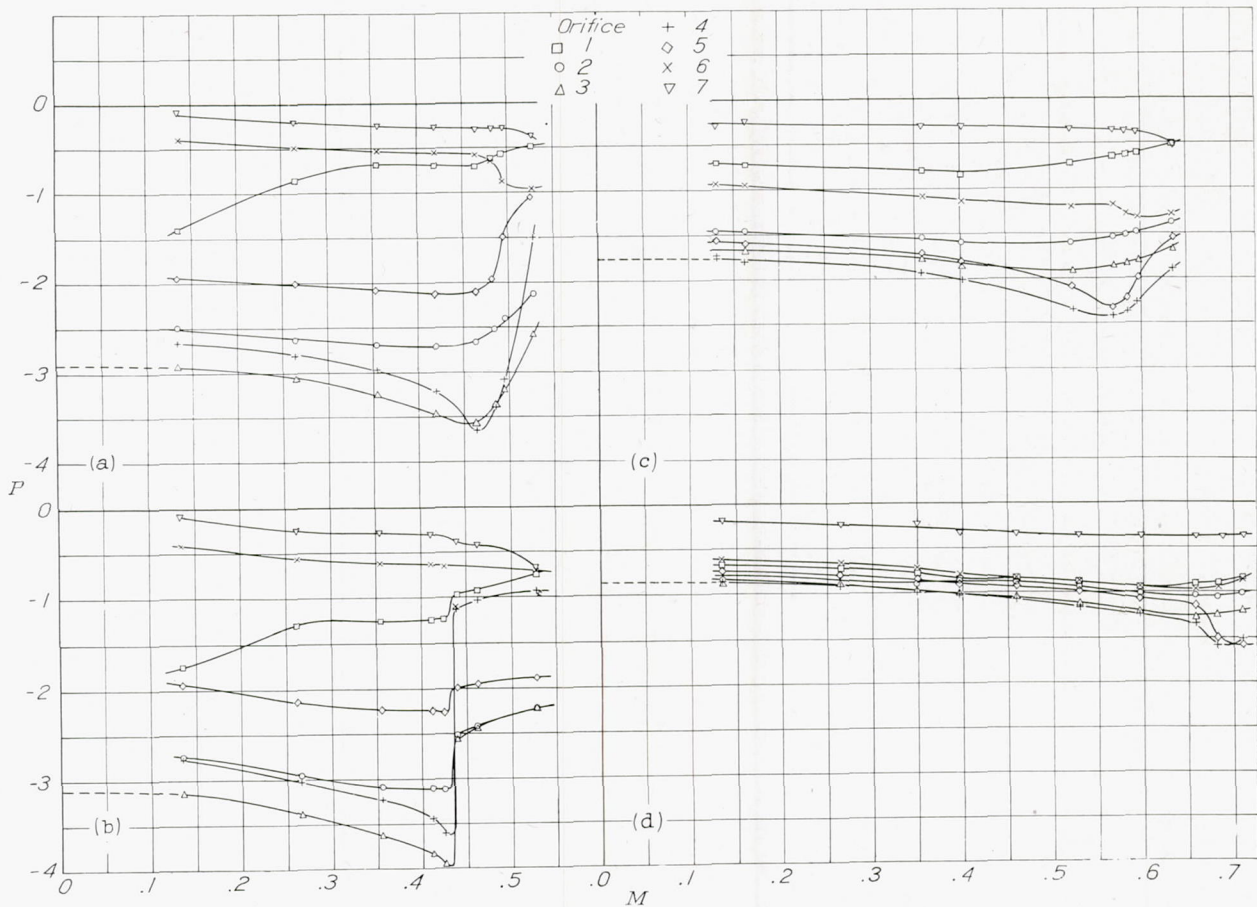
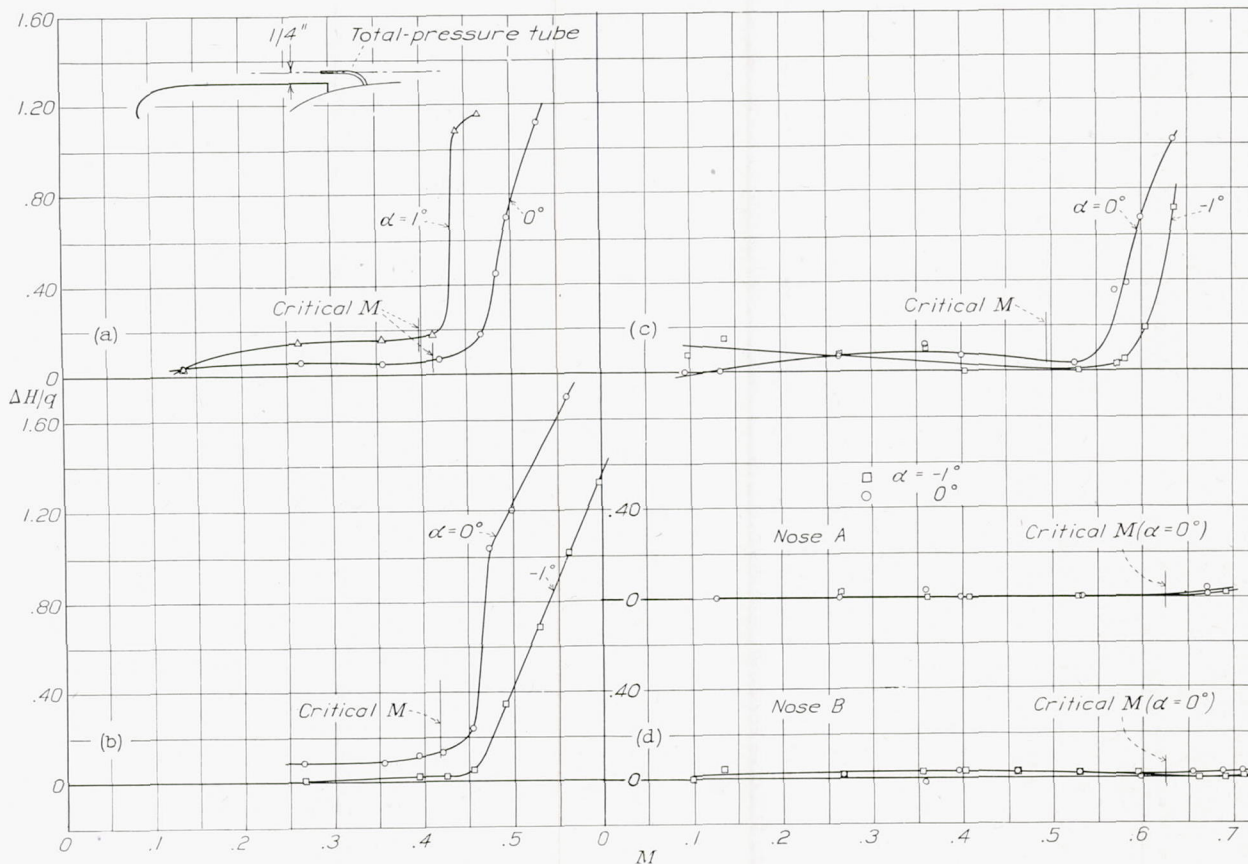


FIGURE 11.—Variation with speed of pressures over top of cowlings.



(a) Nose 4, skirt 1. (b) Nose 5, skirt 2. (c) Nose 7, skirt 1. (d) Noses A and B, skirt 1.

FIGURE 12.—Variation with speed of loss of total pressure in rear of cowlings.

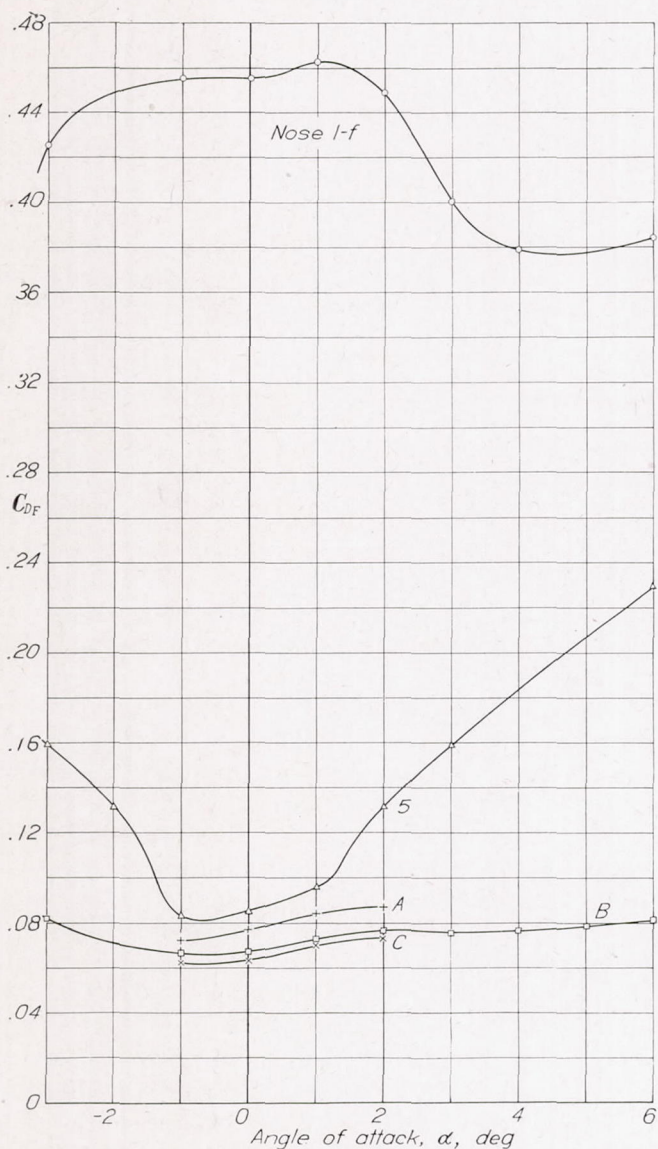


FIGURE 13.—Variation with angle of attack of effective nacelle drag. $M=0.30$.

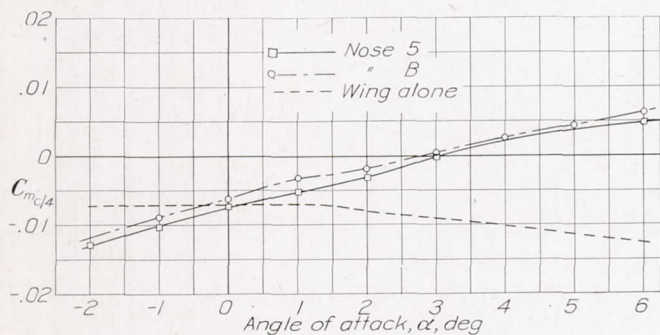


FIGURE 16.—Effect of nacelle on wing pitching moment. Uncorrected for tunnel-wall effects. $M=0.30$.

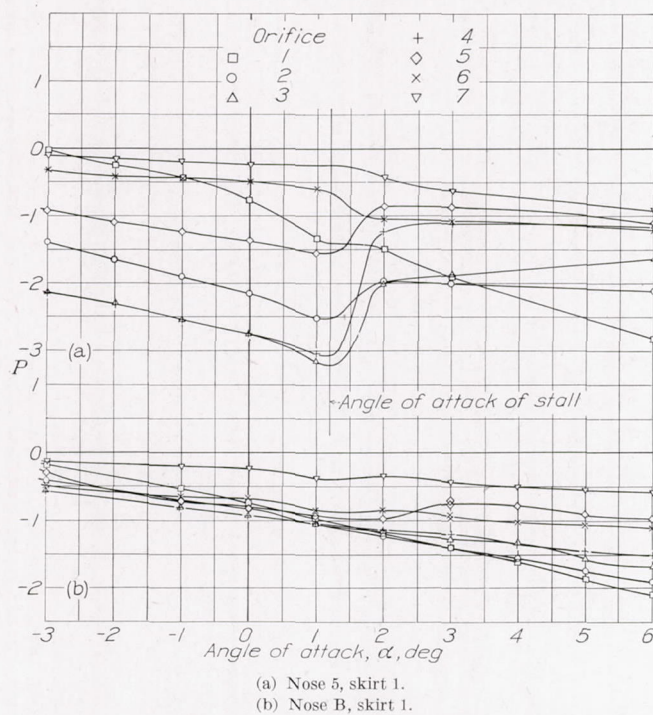


FIGURE 14.—Variation with angle of attack of pressures over top of cowlings. $M=0.30$.

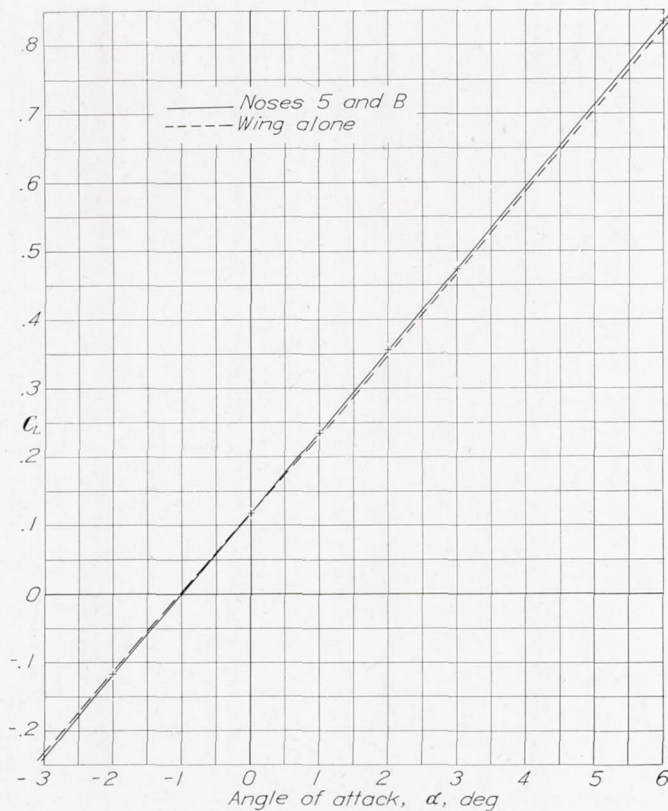


FIGURE 15.—Effect of nacelle on wing lift. Uncorrected for tunnel-wall effects. $M=0.30$.

Cross plots of effective nacelle drag coefficient C_{DF} against angle of attack α for $M=0.30$ are shown in figure 13 for cowling noses 1-f, 5, A, B, and C. The corresponding variation in pressure coefficient P is shown in figure 14 for noses 5 and B.

Figure 15 presents a comparison of the lift curve for the wing-nacelle combination with that of the wing alone. Lift coefficients are based on the wing area of 15.35 square feet:

$$C_L = \frac{\text{lift of wing+nacelle}}{q \times 15.35}$$

There was no measurable difference in lift for the different noses.

Figure 16 shows the effect on wing pitching moment of the presence of the nacelle. The pitching-moment coefficient is based on the wing chord of 2 feet:

$$C_{m_{c/4}} = \frac{(\text{moment of wing+nacelle})_{c/4}}{q \times 15.35 \times 2}$$

The results presented in figures 15 and 16 are uncorrected for tunnel-wall effects and therefore should be used only qualitatively.

COOLING-AIR FLOW

The pressure drop available for cooling across an engine or baffle plate has been shown (reference 3) to be nearly equal to the loss in total pressure between the free stream and the exit opening of the cowling skirt. This loss and the exit speed were measured at only one point in the exit opening of the cowlings under test and, because of the flow variation around the exit opening induced by the presence of the wing, these measurements give only approximations of the conditions existing over the entire cowling. The measured values, however, indicate that the design conductivity K of 9 percent was attained. There was no measurable variation with speed of the $\Delta p/q$ values previously mentioned.

PRECISION

The force-test data presented in this report are uncorrected for tunnel-wall effects. This factor, however, has a negligible influence on the effective nacelle drag owing to the small lift changes involved (see fig. 15) and the small induced drag of a wing spanning a closed tunnel. The effect of the tunnel wall on the critical speed of a body is believed to be of secondary importance when, as in the present case, the cross section of the body is of the order of 1 percent of the cross-sectional area of the jet. The horizontal buoyancy correction for static-pressure gradient is of the order of one-half percent of the effective nacelle drag and is therefore neglected.

The average scatter of the test data for the wing alone and the wing-nacelle combinations indicates random errors in force measurement, based on the wing area, as follows:

$$\begin{array}{ll} C_L \text{-----} \pm 0.003 & C_{m_{c/4}} \text{-----} \pm 0.0005 \\ C_D \text{-----} \pm 0.0001 & M \text{-----} \pm 0.01 \end{array}$$

This error in drag coefficient represents about 4 percent of the effective nacelle drag of nose C, which had the least drag of the models tested. Inasmuch as the same wing drag was subtracted from the drag of each combination, the precision for comparing cowlings is equal to the error just discussed. Absolute values for any cowling will be subject, in addition, to the errors in determining the characteristics of the wing alone and therefore will be subject to errors twice as great.

DISCUSSION

CORRELATION OF DRAG AND PRESSURE-DISTRIBUTION MEASUREMENTS

Figure 7 indicates the speed at which the effective nacelle drag with each cowling increases excessively because of the presence of a compression shock and also the magnitude of the drag change under such conditions. The results indicate that it would be impractical to employ any cowling at flight speeds greater than the speed at which a compression shock forms on the cowling. The bluntest cowlings (4 and 5) are satisfactory for speeds of the order of 300 miles per hour. One of the standard shapes (nose 2) and all of the new shapes developed in this investigation are satisfactory up to about 480 miles per hour (all speeds at sea level, 59° F).

The critical speed at which the local speed of sound was actually reached on each cowling nose has been computed for all the cases in which the peak negative pressure was measured. This speed is shown by a tick on the curves of figures 7 (a) and 7 (c). It is seen that, for noses 2, 4, and 7, the compressibility burble did not occur until the critical speed had been exceeded by about $M = 0.03$; that is, the speed of sound was exceeded locally before a measurable shock occurred on these noses. For noses 5, A, B, and C, the shock apparently formed almost immediately after the critical speed was reached. Since noses 2, 4, and 7 have no common geometric characteristic, the present tests indicate no controlling factor that permits the local speed to exceed the local sonic speed before a compression shock occurs and it must therefore be concluded that any cowling is likely to experience a compressibility burble as soon as the local speed reaches the speed of sound. The critical speed determined on this basis should be used as the upper limit of the flying speed for a radial-engine cowling. The upper limit of the useful speed range for the cowlings tested is then from $M = 0.413$ to $M = 0.625$, or 310 to 480 miles per hour at sea level (59° F).

The speed at which the shock occurred on the wing alone is shown in figure 6 to be only slightly higher than for the combination employing nose C. Wing-nacelle interference probably increases the excess local velocity over that part of the wing adjacent to the nacelle and may slightly reduce the critical speed of the wing in that region. A part of the drag increase beyond the

critical speed shown in figure 7 for nose C, and also for the similar nose shapes A and B, may therefore be due to a shock forming at the wing-nacelle juncture. Although the use of a supporting wing with a higher critical speed would have given a better determination of the speed at which the shock occurred on the cowlings with the highest critical speeds, the wing used (NACA 23012 section) is of conventional thickness and section. Any increase in wing drag caused by a nacelle is properly charged to the effective nacelle drag; the curves of figure 7 therefore indicate correctly the effective nacelle drags associated with the various cowling noses.

As previously discussed, the critical speed V_{cr} in miles per hour is dependent on the atmospheric temperature; that is,

$$V_{cr} = M_{cr} a$$

where

$$a = 33.5 \sqrt{460 + t} \text{ miles per hour}$$

The temperature of the standard atmosphere decreases with altitude to -67° F at about 35,000 feet. The decrease in temperature causes a decrease in the speed of sound a with increasing altitude and results in lower critical speeds as altitude increases. At 30,000 feet the critical speeds for the cowlings tested are lowered to the range of 280 to 430 miles per hour. Since the flying speed of present-day airplanes generally increases with altitude, the danger of encountering serious compressibility effects is very real unless proper care is taken in designing the cowling nose.

As was to be expected, the cowlings with the greatest negative pressure (for example, noses 4 and 5, figs. 10 (c) and 10 (d)) had the lowest critical speeds. Also, as would be expected, the pressure measurements (fig. 10) showed larger peak negative pressures for angles of attack other than zero. The increment due to angle of attack was approximately proportional to the angle change and was greater for cowlings on which the pressure already had a large negative value. The critical speed should be lower, then, when a cowling is pitched or yawed, especially for noses like 4 and 5. The results presented in figures 7 (b) and 7 (c) confirm this conclusion. This behavior illustrates the importance of aligning the cowling with the air direction when the airplane is in the high-speed attitude, especially if the cowling is blunt or is near its critical speed.

The rapid increase in drag with noses 4 and 5 at airspeeds below 200 miles per hour for 2° angle of attack (fig. 7 (d)) is not to be attributed to the compressibility burble. The pressure diagrams (figs. 10 (c) and 10 (d)) show radical changes in pressure distribution and show small peak negative pressures at 2° angle of attack, indicating a flow breakdown; but, from the fact that the maximum local speeds were less than half sonic speed before the change in flow occurred, the breakdown is attributed to ordinary stalling over the top of the cowling and not to a compressibility burble. This effect is discussed in detail later.

The curves of figure 11 show the way in which the static pressure over typical cowlings varies as the speed is increased above the critical speed but fail to show uniform tendencies for all cowlings above the critical M . The blunter cowlings show a decided reduction in the magnitude of the negative pressure coefficients but the reduction occurs at a value of M appreciably higher than the critical value. The cowlings of better shape show a less decided change in pressure coefficient above the critical speed and, in some cases, even an increase in negative pressure (fig. 11 (d)). Figure 10 (j) shows to what extent the pressure distribution may be altered by the compressibility burble. All these results point to the practical conclusion that, if the structural design of a cowling is based on low-speed pressure-distribution data with values suitably increased for compressibility (see fig. 11) to flight speed or critical speed, only a small additional allowance is necessary for the negative pressure developed after the critical speed is exceeded.

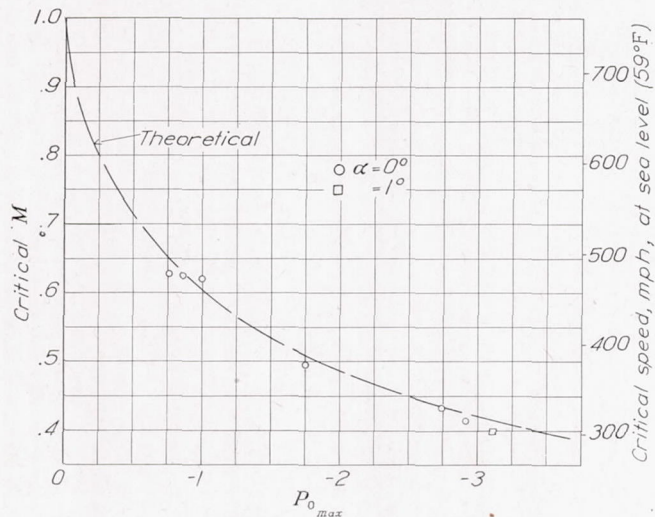


FIGURE 17.—Variation with peak pressure coefficient of critical speed.

The total-pressure measurements of figure 12 also show marked effects for the blunter cowlings and smaller or negligible effects for the cowlings of improved shape. For the blunt cowlings, the loss in total pressure is large and occurs almost immediately after the critical speed is reached; for the improved cowlings, the loss occurs later (fig. 12 (c)) or is of a negligible magnitude (fig. 12 (d)). Thus the total-pressure-tube measurements fail to indicate the occurrence of a shock on the improved cowlings, although the corresponding force measurements show increases in effective nacelle drag with these cowlings. Shocks of a different nature from those recorded for the blunter cowlings, however, may possibly have occurred. If the shocks extended a considerable distance fore and aft, as would be expected from the nearly uniform pressure distributions, their extent normal to the surface may have been small and the wake may have passed under the tube. The

indication is that a detecting tube must be immediately outside the normal boundary layer.

A theoretical relation between peak negative pressure, as measured at low speed, and critical speed has been obtained by Jacobs (reference 4) by defining the critical speed as usual (maximum local speed equal to local speed of sound) and assuming that the negative pressure coefficients increase with speed according to the ratio $1/\sqrt{1-M^2}$. This relation is shown by the curve of figure 17. The measured critical speed for each of the cowlings is plotted in figure 17 against the value of its maximum negative pressure coefficient P_{max} extrapolated to zero speed to give P_{0max} . It is evident that, if the low-speed pressure distribution for a cowling design is known from wind-tunnel or flight tests, the curve of figure 17 may be used to obtain a good approximation of the critical speed of the cowling. The low-speed value of P_{max} must, of course, be for the airplane attitude corresponding to the high speed being investigated.

EFFECT OF VARIATION OF ANGLE OF ATTACK ON FLOW OVER COWLINGS

The negative pressures over the nose of a cowling and the change of pressure with angle of attack are very similar to the pressures and changes experienced by airfoil profiles. Reference 3 points out that the flow direction immediately in front of a cowling is more nearly radial than axial. Depending on the relative direction of the oncoming air and the slope of the cowling just back of the leading-edge radius, a cowling nose may be acting similarly to an airfoil (1) at low or zero lift (noses A, B, C); (2) at high lift (noses 4 and 5); or (3) beyond maximum lift, that is, stalled (nose 1), as shown by the pressure diagrams of figure 10. This comparison indicates the reason why some cowlings have a greater useful angle range without stalling than others.

In the present test set-up, as in the case of actual nacelles near the center of a wing or even of the engine cowling of a single-engine airplane, the relative angle between the oncoming air and the nose of the cowling is increased by the induced upflow in front of the wing. The effective angle of attack of a cowling always being greater than the geometric angle, a cowling may stall at a comparatively small angle in spite of the fact that it is a body of revolution with three-dimensional flow. The likelihood is greater when large negative pressures are present at zero angle.

Figures 10 (c) and (d) show the large negative pressures for noses 4 and 5 at $\alpha=0^\circ$ and the increase of negative pressure with angle. The stall is seen to have occurred before 2° was reached and apparently a negative pressure of about $P=-3.2$ was the most that could be maintained before the stall occurred. (See fig. 14.) Figures 10 (f), (g), and (h) show the small negative pressures for noses A, B, and C at $\alpha=0^\circ$; and figures 10 and 14 indicate that the rate of increase of negative pressure with angle was proportionately

smaller than for noses 4 and 5. If a pressure coefficient P of about -3.2 is still the limit, these cowlings will have a wide useful range of angle of attack without stalling. Figure 13 corroborates these conclusions in indicating a rise in drag for nose 5 outside the range $\pm 1^\circ$, as expected from the stall; whereas the drag of nose B does not rise correspondingly, even at 6° , which was the limit of the tests. Noses A and C undoubtedly have characteristics similar to B. These effects are important not only for controlling the drag of an airplane for cowling attitudes other than zero but also for air scoops or any other construction depending on smooth flow over the top of the cowling.

COMPARATIVE DRAG RESULTS

The results presented in figure 7 indicate no large variation of the effective nacelle drag with speed until the critical speed was reached. The favorable scale effects were balanced at the higher speeds by the unfavorable compressibility effects. The results show, however, appreciable differences in effective nacelle drag for the various nose forms. With nose 5, the effective nacelle drag was approximately 30 percent greater than with nose C. In general, the noses of low curvature, low peak negative pressure, and low local speeds had lower drags and higher critical speeds than those of high curvature and correspondingly high local speeds. The lower skin-friction drag for the models of low local speeds may account in part for the lower drags of noses A, B, and C. A comparison of the pressure-distribution curves for noses 2, A, B, and C (fig. 10) shows the extent to which the peak negative pressures were lowered and the pressure, or the velocity, distribution was made more uniform by successive changes in nose curvature.

The saving in the internal drag due to cooling-flow losses that may be effected by passing exactly the correct quantity of cooling air through a cowling at every speed instead of using openings and exits of fixed size for the entire speed range have been previously discussed (reference 3). The results presented by figure 18 show the drag reduction due to changing the exit opening from 0.25 inch to 0.11 inch. The fact that the cowling with the smaller exit opening (skirt 2) shows a lower critical speed at $\alpha=0^\circ$ suggests that a part of the air which formerly passed inside the cowling (with the larger exit opening) now passes outside the cowling to increase the local speed on the cowling nose. The increased speed outside the cowling, or the equally important factor of increasing angle of relative wind at the cowling nose with reduced flow through the cowling, also appears as a detrimental effect in reducing the useful angle-of-attack range of a cowling. With nose 5, the cowling stalled at 1° . (Cf. figs. 10 (d) and 10 (i).) Both the lower critical speed and the smaller useful angle-of-attack range emphasize the relative importance of using the best possible nose shape when the internal flow is most restricted, as is the case in

high-speed flight with the optimum amount of cooling air.

Both the effective nacelle drag for nose 1 (fig. 8) and the pressure distribution (fig. 10 (a)) indicate that this nose was stalled at all angles of attack, including 0° . An attempt was made to improve the flow over the nose by successively cutting back the nose to form profiles with circular arcs of larger radii inscribed in the lead-

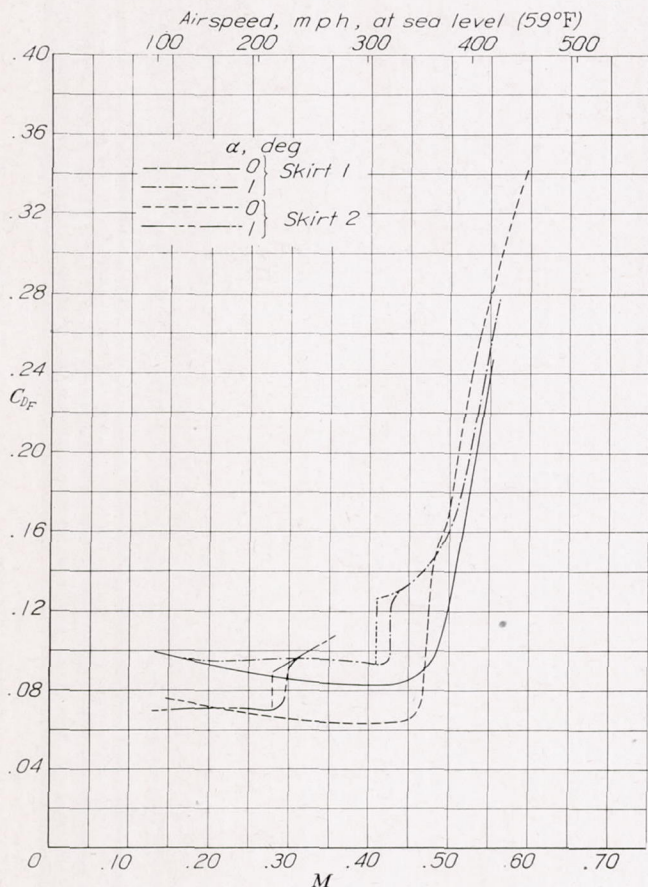


FIGURE 18.—Comparison of effective nacelle drag of nose 5 with skirt 1 and skirt 2.

ing edge on the assumption that a radius would be reached at which the flow would be unstalled. The drag for each modification, however, was found to be larger than for the preceding condition. The change in drag with increase of angle of attack for nose 1-f, as shown in figure 13, indicates that the decrease in effective angle of attack on the bottom of the cowling caused a considerable improvement in the flow at that point which was not at first counteracted by increased severity of the stall on top of the cowling. The modi-

fications to nose 1 were ineffective, probably because the slope of the chord line of the nose decreased as the nose radius was increased. In critical cases, it appears to be much more important to align the slope of the nose with the relative wind than to increase the nose radius.

CONCLUSIONS

1. The Mach numbers at which the effective nacelle drag abruptly increased owing to the compressibility burble ranged from 0.41 to 0.63 (310 to 480 miles per hour at sea level (59° F)) for the conventional cowlings tested. Because of the decrease in the speed of sound with decreasing temperature, the corresponding range at 30,000 feet altitude (-48° F) would be 280 to 430 miles per hour.

2. The effective nacelle drag increased so rapidly beyond the critical speed that flight at speeds above the critical speed of the cowling would be impractical.

3. The pressure distribution over any cowling nose, as measured in flight at moderate speeds or in a wind tunnel at low speed, may be used to predict the critical speed of the nacelle.

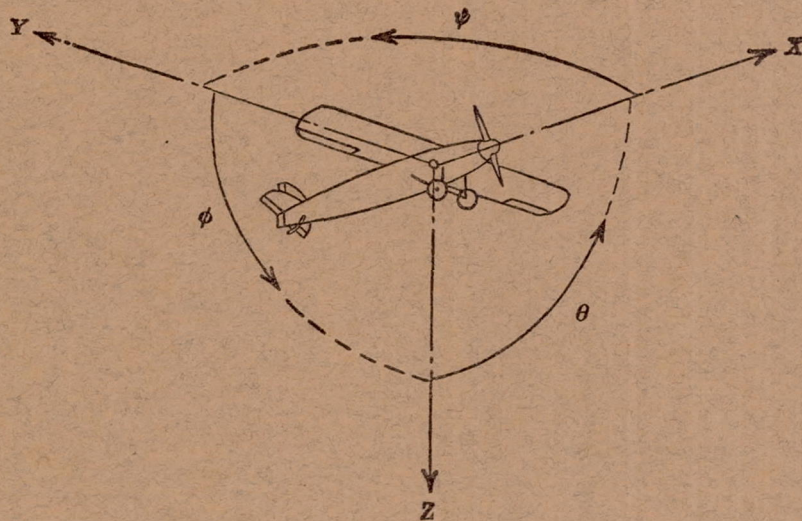
4. The criterion for a conventional-type cowling designed to have a high critical speed appears to be low uniform negative pressures over the nose. This condition indicates a speed over the entire nose that is constant and exceeds the general stream speed by a minimum amount.

5. The cowlings developed to have the highest critical speeds also had the lowest drags throughout the entire speed range and had a greater useful angle-of-attack range without an increase in drag.

LANGLEY MEMORIAL AERONAUTICAL LABORATORY,
NATIONAL ADVISORY COMMITTEE FOR AERONAUTICS,
LANGLEY FIELD, VA., March 30, 1939.

REFERENCES

1. Stack, John: The Compressibility Burble. T. N. No. 543, NACA, 1935.
2. Lindsey, W. F.: Drag of Cylinders of Simple Shapes. Rep. No. 619, NACA, 1938.
3. Theodorsen, Theodore, Brevoort, M. J., and Stickle, George W.: Full-Scale Tests of N. A. C. A. Cowlings. Rep. No. 592, NACA, 1937.
4. Jacobs, Eastman N.: Methods Employed in America for the Experimental Investigation of Aerodynamic Phenomena of High Speeds. Misc. Paper No. 42, NACA, 1936.
5. Robinson, Russell G.: Sphere Tests in the N. A. C. A. 8-Foot High-Speed Tunnel. Jour. Aero. Sci., vol. 4, no. 5, March 1937, pp. 199-201.



Positive directions of axes and angles (forces and moments) are shown by arrows

Axis		Force (parallel to axis) symbol	Moment about axis			Angle		Velocities	
Designation	Symbol		Designation	Symbol	Positive direction	Designation	Symbol	Linear (component along axis)	Angular
Longitudinal-----	X	X	Rolling-----	L	Y→Z	Roll-----	φ	u	p
Lateral-----	Y	Y	Pitching-----	M	Z→X	Pitch-----	θ	v	q
Normal-----	Z	Z	Yawing-----	N	X→Y	Yaw-----	ψ	w	r

Absolute coefficients of moment

$$C_l = \frac{L}{qbS}$$

(rolling)

$$C_m = \frac{M}{qcS}$$

(pitching)

$$C_n = \frac{N}{qbS}$$

(yawing)

Angle of set of control surface (relative to neutral position), δ . (Indicate surface by proper subscript.)

4. PROPELLER SYMBOLS

D Diameter

p Geometric pitch

p/D Pitch ratio

V' Inflow velocity

V_s Slipstream velocity

T Thrust, absolute coefficient $C_T = \frac{T}{\rho n^2 D^4}$

Q Torque, absolute coefficient $C_Q = \frac{Q}{\rho n^2 D^5}$

P Power, absolute coefficient $C_P = \frac{P}{\rho n^3 D^5}$

C_s Speed-power coefficient = $\sqrt[5]{\frac{\rho V_s^5}{P n^2}}$

η Efficiency

n Revolutions per second, rps

Φ Effective helix angle = $\tan^{-1}\left(\frac{V}{2\pi r n}\right)$

5. NUMERICAL RELATIONS

1 hp = 76.04 kg-m/s = 550 ft-lb/sec

1 metric horsepower = 0.9863 hp

1 mph = 0.4470 mps

1 mps = 2.2369 mph

1 lb = 0.4536 kg

1 kg = 2.2046 lb

1 mi = 1,609.35 m = 5,280 ft

1 m = 3.2808 ft